mathematics

MDPI

Article

Q Factor Enhancement of Open 2D Resonators by Optimal Placement of a Thin Metallic Rod in Front of the Longitudinal Slot

Elena D. Vinogradova * and Paul D. Smith

School of Mathematical and Physical Sciences, Macquarie University, Sydney 2109, Australia
* Correspondence: elena.vynogradova@mq.edu.au

Abstract: A rigorous approach was employed for the accurate evaluation of the electromagnetic interaction between a thin metallic rod and a two-dimensional (2D) slotted cavity. The problem was posed as a classical boundary value problem for the Helmholtz equation in which a 2D slotted open cavity is bounded by an arbitrary but otherwise smooth contour with a longitudinal slit. Using the *method of analytical regularization*, the problem was transformed to well-conditioned coupled infinite systems of linear algebraic equations for the Fourier coefficients in the expansions of induced surface currents on the rod and slotted cavity. When truncated to finite size, their solutions exhibit fast convergence to the exact solution as the order is increased. This feature makes it possible to investigate the spectral and scattering characteristics of the coupled cavity and rod to within any desired accuracy. In this paper, the complex eigenvalues for a slotted cavity in the presence of a thin rod and the dependence upon their relative location were investigated, particularly to find where there is significant or optimal enhancement of the *Q* factor. Such optimisation may be exploited in the design of advanced slot antennas and slotted waveguides.

Keywords: open cylindrical cavities in presence of the wires; rigorous method of analytical regularization solution; complex *TM* oscillations; complex eigenvalues; enhancement of the *Q* factor

MSC: 78-10; 78M50; 65F22

Citation: Vinogradova, E.D.; Smith, P.D. *Q* Factor Enhancement of Open 2D Resonators by Optimal Placement of a Thin Metallic Rod in Front of the Longitudinal Slot. *Mathematics* **2022**, *10*, 2774. https://doi.org/10.3390/math10152774

Academic Editor: Nikolaos Tsitsas

Received: 1 May 2022
Accepted: 25 July 2022
Published: 4 August 2022

1. Introduction

Thin metallic rods or wires are often used for tuning slotted resonators and waveguides. There are a vast number of publications related directly or by implication to this subject. Our focus was the methods of solution applied, of which the following examples are representative. The electromagnetic field (EMF) coupling to a loaded thin wire in a cylindrical/coaxial cavity was investigated in [1]. The coupling of the cavity field to the wire was determined from an analysis of a distributed voltage and current source model based on transmission line theory as well as via coupled integral equation techniques. Electromagnetic field coupling to a thin wire, located symmetrically inside a rectangular enclosure, was examined in [2]. This paper calculated, for a conductor inside a cavity, the current which was induced by lumped and distributed sources. The current was obtained both analytically (Green's function method) and numerically (multilevel fast multipole method). Energy coupled mode theory (ECMT) employs a coupled mode equation in the frequency domain. In [3], the authors, using the method of images, extended it to deal with important cases where resonators are in close proximity to conducting surfaces. Evaluation of the current induced on a wire within a resonant cavity, illuminated by a plane wave through one or several apertures, was performed in [4]. The electric field distribution inside the rectangular enclosure, obtained by using two circuit models, was then introduced as the excitation of the line on the basis of Taylor's model. Similar problems have been studied, for example, in [5–8]; although the list of publications in the field is extensive, most papers have relied on the methods already mentioned or their variants in the papers already cited—these are fully representative of current approaches to the problem under study.

In this paper, we present a completely different and highly accurate method to study the electromagnetic interaction between a thin metallic rod and a 2D slotted cavity. The goal of our investigation was the construction of a model which possesses a full theoretical justification for the provably accurate evaluation of coupling between the resonant cavity and tuning element, shaped as a thin metallic circular cylinder. Moreover, that accuracy, which can be prescribed in advance, could be achieved in practice. This resulted from employing the method of analytical regularization (MAR). The guarantee of accuracy derives from the final form of equations obtained after application of the MAR. The final form of our solution fully met the criteria laid out in the survey [9] of mathematical foundations for error estimation; it thus may be described as being of benchmark quality.

By contrast, all the other methods previously mentioned (such as the methods of moments, and so on) lack theoretical bases for guaranteeing accuracy or convergence as described in [9]. Standard formulations of scattering and diffraction problems usually prefer integral equations for the unknown surface densities because the unknowns are reduced in dimension and the Sommerfeld radiation condition is automatically incorporated. Structures containing apertures or cavities result in integral equations of the first kind. Difficulty arises when discretisation and other purely numerical techniques are employed, where the matrix of the system becomes more and more ill-conditioned as the discretisation is increasingly refined, and especially near sharp resonances, its numerical solution increasingly diverges markedly from the true solution. This behaviour is an unavoidable artifact of first kind integral equations. The MAR transforms such ill-posed first kind equations (and systems of equations equivalent to such) to a second kind system (usually in infinite matrix form) for which the standard numerical approach employing truncation methods is guaranteed to converge. It removes the uncertainty, or instability, inherent in numerical solutions to first kind systems.

The 2D slotted cavity is discussed from two points of view. First, we calculated accurately the perturbation induced by the rod, located outside the cavity, on the non-perturbed complex eigenvalues of the *TM* modes that potentially exist in the isolated slotted cavity (in the absence of the rod). It was found that a suitable location of the rod relative to the open cavity, along with an appropriate choice of rod thickness, had the striking effect of a huge enhancement in the Q factor. Secondly, we calculated the resonant currents induced by an obliquely propagating plane wave at the surfaces of the rod and cavity. Results are presented for slotted circular and rectangular cavities in the presence of the rod (or wire).

The method we used was not formulated in terms of the more usual concepts employed in the theory of electromagnetic coupling, such as "coupling coefficients", "inductive (capacitive) coupling", "electrical (magnetic) walls", and so on; neither did it not use any of the approaches developed in [1–8] and other related publications. Although it is rather infrequently used nowadays, we used a classical approach to the solution of the problem. We considered a mixed boundary value problem for Maxwell's equations, starting from its mathematically correct statement and incorporating all conditions that ensure *uniqueness* of the solution. Fulfilment of these conditions led to the emergence of coupled surface integral equations, which as indicated above, were of the first kind and ill-conditioned, and thus requiring regularization for any calculations of moderate to high accuracy. Their transformation to a set of well-conditioned equations was achieved by employing the *method of analytical regularization* (MAR), the basic ideas of which have been described in detail in [10,11]. There are several versions of MAR equivalent to [10,11]. One of them is based on the projection of these singular integral equations to the set of weighted Chebyshev polynomials, which are the orthogonal eigenfunctions of the singular (static) part of the integral equation operator. Equivalently, such a projection can be performed in the Fourier transform domain using the transforms of the Chebyshev polynomials [12]. The other equivalent approach is based on the discrete Fourier transform and analytical inversion of the associated Riemann–Hilbert problem [13].

A schematic description of the solution obtained and the geometry of the structures examined in this paper are given in Section 2. In Section 3, the structure of a slotted circular

cavity in the presence of a circular rod is studied, whilst in Section 4, a slotted rectangular cavity with a circular rod is considered. Concluding remarks are presented in Section 5.

All computations in this paper were done on a standard modern PC. We used the MATLAB environment for the computations, employing its standard packages for matrix inversion, fast Fourier transform, and graphical post-processing of the data. It is worth emphasizing that the algorithms for the matrix operations performed by the software in the solution of system (4) are reliable and minimally affected by roundoff and other errors precisely because the matrices are well-conditioned. Ensuring this is the key reason why the MAR was employed.

2. Problem Geometry and Schematic Description of the Solution

The general geometry of the problem is shown in Figure 1a. An *E*-polarized plane wave obliquely propagating at an incident angle α strikes a slotted cavity and rod, both of arbitrary profiles. The particular case when both the metallic cavity and rod are of circular shape (of radii r_1 and r_2, respectively) is shown in Figure 1b. Another particular case of the slotted rectangular cavity (sides a and b, $b > a$,) in the presence of a circular rod is shown in Figure 1c. There is no restriction on the location of the center (x_0, y_0) of the arbitrary solid cylinder: it may be placed inside or outside the cavity. There are no restrictions on the slit widths, $2r_1\varphi_1$ (Figure 1b) or w (Figure 1c), or on the relative wave numbers, kr_1 (Figure 1b) or kb (Figure 1c).

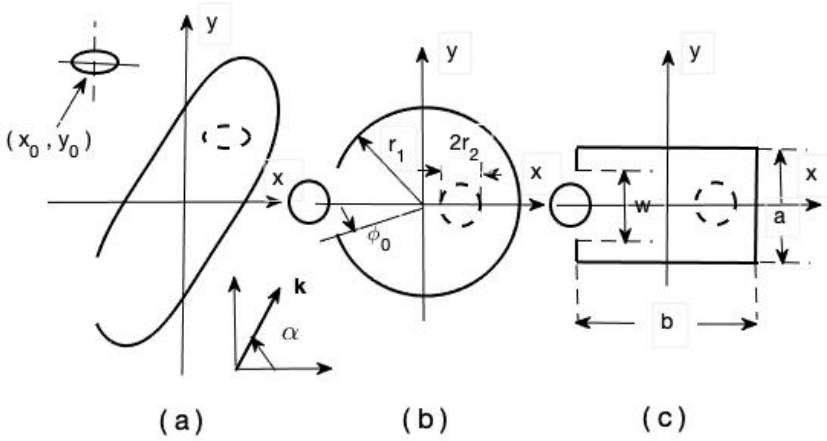

Figure 1. Problem geometry: (**a**) slotted cavity and rod (centre (x_0, y_0)), both of arbitrary shape; (**b**) slotted circular cavity and circular rod (wire); (**c**) slotted rectangular cavity and circular rod (wire). Some alternative locations of the rod are shown in dashed line.

A comprehensive treatment of the rigorous solution and its deduction using the MAR for isolated 2D arbitrary hollow cylinders with longitudinal slits were presented in [14]; it was subsequently used to analyse the scattering of an *E*-polarized plane wave by a rectangular cavity with finite flanges [15]. The determination of the complex eigenvalues with any prescribed accuracy for arbitrary slotted two-dimensional cavities is also based on the MAR. The efficacy of this approach was demonstrated in [16], where the first fifteen complex eigenvalues of various slotted elliptical cavities (with different eccentricities and variably placed longitudinal slits) were calculated with an accuracy of eight significant decimal digits.

Multiple backscattering of an *E*-polarized plane wave by a double-layered array of infinitely long cylinders was also treated by the MAR [17]. Mixed boundary value problems for the Laplace equation, incorporating multiple conductors, were investigated by the same method with particular applications to impedance calculations for transmission lines with an adjustable inner conductor [18]. The theoretical advances achieved in these cited papers where the MAR has been employed means that the theoretical part of this paper may be subsumed as a particular case of general theory and application of the MAR; we may therefore restrict ourselves to a briefer and somewhat schematic description.

We considered the diffraction of an E-polarized plane wave by a 2D slotted cavity in the presence of a metallic rod located outside the cavity. There were no restrictions on the parameters of the problem, including slit width, as well as relative electrical size of the cavity (r_1/λ). The problem was formulated in terms of the longitudinal electric component E_z of the electromagnetic field. According to the superposition principle, we may seek the scattered field E^{sc} as the sum of two contributions from the cavity and the rod. Following classical potential theory, each contribution is represented as a single-layer potential employing the individually specified surface current densities on those structures. Enforcing the boundary conditions leads to two coupled first kind integral equations, which, after expansion of the surface current densities in Fourier series, are concisely representable in operator form as

$$\begin{aligned} I_{11}X + I_{12}Y &= B_1 \\ I_{21}X + I_{22}Y &= B_2 \end{aligned} \tag{1}$$

where I_{ij} $(i,j = 1,2)$ are the problem operators. The off-diagonal operators I_{12} and I_{21} represent the influence of the rod on the cavity surface currents and of the cavity surface on the rod currents, respectively; the diagonal operators I_{11} and I_{22} represent the self-interaction on the cavity surface and the rod, respectively. The quantities $X = \{X_n\}_{n=0}^{\infty}$ and $Y = \{Y_n\}_{n=0}^{\infty}$ represent unknown vectors of the Fourier coefficients to be found; $B_1 = \{B_{1,n}\}_{n=0}^{\infty}$ and $B_2 = \{B_{2,n}\}_{n=0}^{\infty}$ are known vectors of the Fourier coefficients generated by the propagating plane wave. Obtaining Equation (1) is a routine procedure, after which most papers consider the deduction of the solution to be complete for subsequent numerical investigations.

However, it is well-known that the first kind equations of type (1) are ill-conditioned and numerical algorithms based on this equation are prone to numerical catastrophe, unavoidably so in dealing with structures of the type considered in this paper, where resonant effects of at least moderate strength may be anticipated. As indicated in the Introduction, the MAR transforms Equation (1) into well-conditioned matrix equations of the second kind; such equations are readily amenable to highly accurate numerical solution.

Briefly, the transform is realised in the following way. First, the operators I_{11} and I_{22}, each containing a singularity of logarithmic type, are split into singular I_{11}^s and I_{22}^s and regular I_{11}^r and I_{22}^r parts with $I_{11} = I_{11}^s + I_{11}^r$ and $I_{22} = I_{22}^s + I_{22}^r$ so that Equation (1) takes the form

$$\begin{aligned} \left(I_{11}^s + I_{11}^r\right)X + I_{12}Y &= B_1 \\ I_{21}X + (I_{22}^s + I_{22}^r)Y &= B_2 \end{aligned} \tag{2}$$

The next stage is to find (or construct) the respective inverse operators $\left(I_{11}^s\right)^{-1}$ and $(I_{22}^s)^{-1}$ of the singular operators I_{11}^s and I_{22}^s. It should be emphasised that the construction of the inverse operators is realised *analytically*. The general theory of the *analytical* construction of the inverse operators is described in detail in [10,11]. Specific details related to construction of the inverse operators in the case of wave scattering problems, and which are relevant to the present paper, can be found in [14]. This procedure uses the mathematical apparatus of the Abel integral transform, or the theory of operators of fractional integration and differentiation, described in detail in [10]. The term 'analytical' in the so-called *method of analytical regularization* distinguishes it from various other and widely used methods of *numerical* regularization.

Once the analytically constructed inverse operators are obtained, application to both sides of Equation (2) produces

$$\begin{aligned} \left(I_{11}^s\right)^{-1}\left(I_{11}^s + I_{11}^r\right)X + \left(I_{11}^s\right)^{-1}I_{12}Y &= \left(I_{11}^s\right)^{-1}B_1 \\ (I_{22}^s)^{-1}I_{21}X + (I_{22}^s)^{-1}(I_{22}^s + I_{22}^r)Y &= (I_{22}^s)^{-1}B_2 \end{aligned} \tag{3}$$

After inversion of the singular parts of Equation (3), we obtain well-conditioned coupled infinite systems of the second kind in the form

$$\begin{aligned}(I + H_{11})X + H_{12}Y &= \hat{B_1}\\ H_{21}X + (I + H_{22})Y &= \hat{B_2}\end{aligned} \tag{4}$$

In Equation (4), I is the identity operator, the operators $H_{11} = \left(I_{11}^s\right)^{-1} I_{11}^r$, $H_{12} = \left(I_{11}^s\right)^{-1} I_{12}$, $H_{21} = \left(I_{22}^s\right)^{-1} I_{21}$, and $H_{22} = \left(I_{22}^s\right)^{-1} I_{22}^r$ are completely continuous (compact) operators on the functional space l_2 of square-summable sequences, and $\hat{B_1} = \left(I_{11}^s\right)^{-1} B_1$, $\hat{B_2} = \left(I_{22}^s\right)^{-1} B_2$ are known modified right-hand side vectors, belonging to the same class l_2.

Being of second kind, the Fredholm alternative is applicable, and hence, Equation (4) is soluble by the truncation method. The fast convergence of the successive solutions of the truncated systems to the exact solution as the truncation order is increased has been demonstrated for similar systems of equations in the papers [14–16]. However, because we wished to investigate delicate effects related to perturbations of the complex eigenvalues of the complex oscillations in the slotted cavity as the position of the metallic rod varies, it was beneficial to make some estimates of the accuracy of the computations when the truncation method was used for the structures shown in Figure 1. For this purpose, it was convenient to use the dependence of the *normalized truncation error* $e(N) \equiv e_N$ upon truncation number N, treated in the maximum l_2-norm sense

$$e(N) \equiv e_N = \frac{max_n \left| x_n^{N+1} - x_n^N \right|}{max_n \left| x_n^{N+1} \right|} \tag{5}$$

Here, x_n^N, $n = 0, \ldots, 2N+1$ denotes the components of the vector $\{X_n\}_{n=0}^N \cup \{Y_n\}_{n=1}^N$ representing the solution at truncation level N, while x_n^{N+1} denotes the components at truncation level $N+1$. The typical behaviour of e_N for a slotted circular cavity at three different relative locations of the rod, $x_0/r_1 = -5, -1.5, -1.15$, and two slit widths, $w/r_1 = 0.5176,\ 1$, is shown in Figure 2.

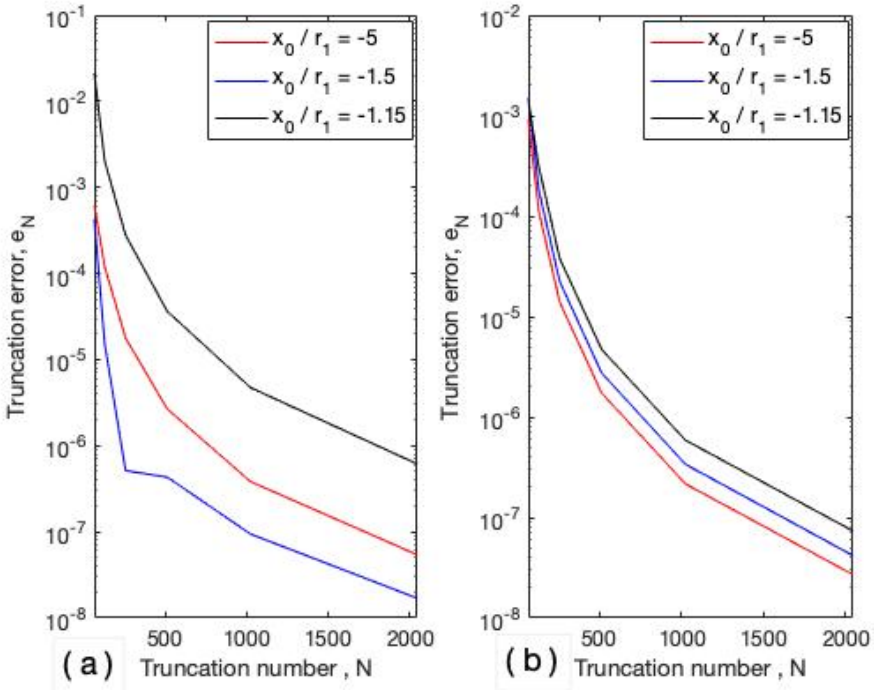

Figure 2. Relative truncation error e_N versus truncation number N for a slotted circular cavity at the different relative locations x_0/r_1 of the rod, $r_2/r_1 = 0.1$, $kr_1 = 2\pi$ (so $r_1 = \lambda$), with slit widths: (**a**) $w/r_1 = 2\sin\pi/12 \approx 0.5176$; (**b**) $w/r_1 = 2\sin\pi/6 = 1$.

The calculation of the function e_N was carried out with a much extended range of truncation numbers N with the purpose of justifying the capability of the MAR to calculate the *complex eigenvalues* with an accuracy of 6–8 significant decimal digits. It can be seen from the plots of e_N in Figure 2 that when the rod approaches the slit ($x_0/r_1 = -1.15$), its value rapidly drops because of a strong interaction between the slit and rod. A similar behaviour of the value e_N is observed for the rectangular cavity–rod interaction.

3. Influence of the Circular Rod on Resonance Characteristics of the Circular Cavity with Longitudinal Slit When Placed Outside

This section investigates the influence of the rod on the spectral characteristics of the slotted circular cavity, addressing the question: how does the rod perturb the complex eigenvalues of the isolated open cavity? A second problem concerns the distinction between the resonance scattering of an isolated cavity and that of the cavity coupled with the metallic rod. These two problems are closely related and should be analysed jointly. For the calculations of this Section, we extracted, from the spectrum of the complex eigenmodes of the slotted circular cavity published in [16], the first three: TM_{c01}, TM_{c11}, and TM_{s11}, with corresponding complex eigenvalues γ_{c01}, γ_{c11}, and γ_{s11}, respectively (using the notation $\gamma_{c(s)nm} = \gamma'_{c(s)nm} - i\gamma''_{c(s)nm}$ for real and imaginary parts). As noted in [16], the indices n and m stand for the number of EMF variations along the angular (ϕ) and radial (ρ) coordinates, respectively. The indices "c" and "s" are attributed to symmetric ("cosine") and anti-symmetric ("sine") oscillations, respectively. The complex eigenvalues of the isolated cavity extracted from [16] are shown in Table 1; we refer to them as "non-perturbed" eigenvalues.

Table 1. Selected complex eigenvalues of the open circular cavity.

w/r_1 \ $\gamma_{c(s)nm}$	γ_{c01}	γ_{c11}	γ_{s11}
$2\sin\frac{\pi}{12} = 0.5176$	$2.380492 - i0.002975$	$3.745509 - i0.026426$	$3.831095 - i0.000008126$
$2\sin\frac{\pi}{6} = 1$	$2.301132 - i0.052355$	$3.592331 - i0.291395$	$3.819451 - i0.002146$

In calculating complex eigenvalues, we used a straightforward approach, which was possible only because the MAR possesses fast convergence of its truncated solutions (see Figure 2). The algorithm for finding the complex eigenvalues is, with some simplifications, as follows. We considered the homogeneous equation obtained from (4) by nulling its right-hand sides, i.e., $\hat{B}_1 = \hat{B}_2 \equiv 0$. This equation may be symbolically represented as $AZ = 0$, $Z = \{X \cup Y\}$, where A is the infinite dimensional matrix of Equation (4). It possesses non-trivial solutions if and only if its determinant equals zero, i.e., $\det A = 0$. The complex-valued roots of this *characteristic equation* are the complex eigenvalues of the electromagnetic boundary value problem. To find the complex eigenvalues, we used the truncated version of this equation, $\det A_N = 0$, where A_N is the truncated matrix and N is the truncation number. The numerical routine includes finding the complex eigenvalue $\gamma_{c(s)nm}$ at some initial fixed value N_0 and its successive refinements at larger values $N > N_0$ until the prescribed or required accuracy of calculation of $\gamma_{c(s)nm}$ is achieved. As an example, let us calculate the complex eigenvalue γ_{c01} for the TM_{c01} mode, which develops in an open circular cavity with a rod outside the cavity, when $r_2/r_1 = 0.05$, $x_0/r_1 = -1.15$, and $w/r_1 = 2\sin\pi/12 \approx 0.5176$.

The estimates $\gamma_{c01}^{(N)}$ for this complex eigenvalue γ_{c01} at truncation number N are shown in Table 2.

The calculations revealed that even the lowest value $N = 128$ provided enough accuracy for radio engineering practice. The computational time t_c for $N = 128$ was measured in fractions of a second (in general, $t_c < 1$ s). When $N = 256$, the computational time lay between two and five seconds. From a practical point of view, further increments in N were not necessary, and because of this, we used the truncation value $N = 256$ in calculating the plots.

Table 2. Accuracy of calculation of the complex eigenvalue $\gamma_{c01}^{(N)}$ at truncation number N.

Truncation Number N	Estimates of γ_{c01}
128	**2.381**368254677136 − i**0.000557**776464831
256	**2.381372**093234430 − i**0.000557690**684937
512	**2.381372**588189465 − i**0.000557679**205314
1024	**2.381372652**204457 − i**0.000557677**663617
2048	**2.381372660**445512 − i**0.000557677**458989
4096	**2.381372661**506500 − i**0.000557677**431874

The bold demonstrate the converrgence explicitly.

To gain more insight into the influence of the rod as its position along the x-axis varies, we calculated the Q factor Q_{c01} of the complex eigenmode TM_{c01} versus the relative location of the rod x_0/r_1 in the intervals $x_0/r_1 \in (-5, -1-2r_2/r_1) \cup (-1+2r_2/r_1, 1-2r_2/r_1) \cup (1+2r_2/r_1, 5)$ for two values of the relative rod radius, $r_2/r_1 = 0.01,\ 0.025$. These two dependences $Q_{c01}(x_0/r_1)$ are shown in Figure 3. The Q factor was calculated from its standard definition, $Q_{c(s)nm} = -Re\ \gamma_{c(s)nm}/2\ Im\ \gamma_{c(s)nm}$.

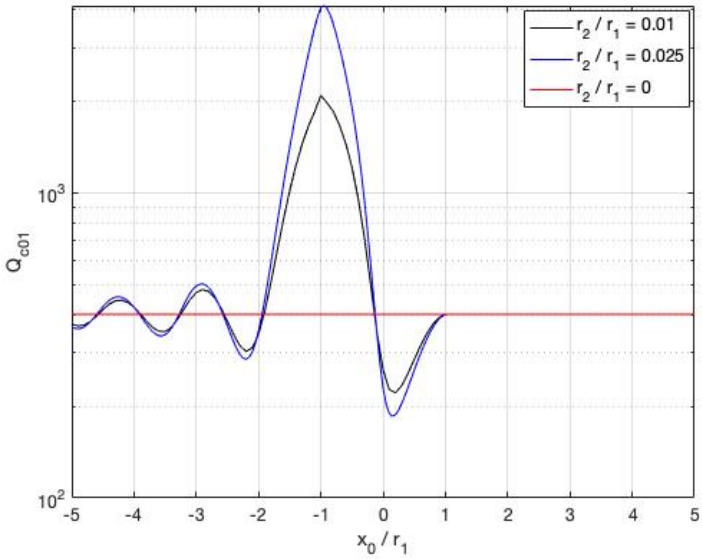

Figure 3. Q factor (Q_{c01}) versus relative distance x_0/r_1 for two values of the rod radius $r_2/r_1 = 0.01,\ 0.025$, slit width $w/r_1 = 2\sin\pi/12 \approx 0.5176$.

Analysing the behaviour of $Q_{c01}(x_0/r_1)$, one may recognise that the influence of the rod is negligible when $1 + 2r_2/r_1 \leq x_0/r_1 \leq 5$. The reason is simply explained: from both geometrical and electromagnetic points of view, the rod is well-shielded by the back side of the cavity and does not directly interact with the slit. On the other hand, when the rod is positioned in the interior of the cavity, near the back wall, two phenomena are observed as it is moved towards the aperture. First, the value of $Q_{c01}(x_0/r_1)$ drops at the point of maximum electromagnetic field intensity of the TM_{c01} mode. For the closed cavity, the maximum lies at the point $(0, 0)$, but for the slotted cavity, the maximum intensity is slightly shifted in the positive direction of the x-axis, lying at a point $(0, \delta), \delta \ll 1$. Placement of the rod at this point (a wave crest) causes maximum distortion and hence a significant decrease in the value $Q_{c01}(\delta/r_1)$. After passing through this point and approaching the slit, the rod starts to overlap or partially block the slit. The strong interaction with the slit lowers the radiation losses, leading to a significant enhancement in the value of Q_{c01}, the maximum value of which occurs when the rod is placed exactly at the middle of the slit ($x_0 = -1 + \sqrt{1 - (w/2)^2}$). Similar considerations apply when the rod is placed outside the cavity but in the proximity of the slit.

In what follows, we distinguish between the term "wires" and "thin circular cylinders", according as $r_2/r_1 \leq 0.01$ or $r_2/r_1 > 0.01$. The dependences $Q(x_0/r_1)$ for the symmetric eigenmodes TM_{c01}, TM_{c11} and for the non-symmetric eigenmode TM_{s11} in the interval $-3 \leq x_0/r_1 \leq -1 - r_2/r_1$ are shown in Figures 4 and 5, respectively. The difference in the influence of the wire on symmetric and anti-symmetric eigenmodes of the isolated slotted cavity is striking. The symmetric eigenmodes are highly sensitive to the presence of the wire whereas the non-symmetric mode is not. From a physical point of view, this phenomenon is explained by the difference in the EMF distribution inside the cavity for symmetrical and anti-symmetrical eigenmodes. For the symmetric eigenmodes, the wave crests always face the slit and hence the wire or rod. The wire interacts with the high intensity electromagnetic field, causing maximal perturbation. By contrast, for anti-symmetric eigenmodes, the minima of the *EMF* distribution are located right in front of the slit, so the interaction with the wire is weak. Comparison of the plots in Figures 4 and 5 clearly reveals this fact.

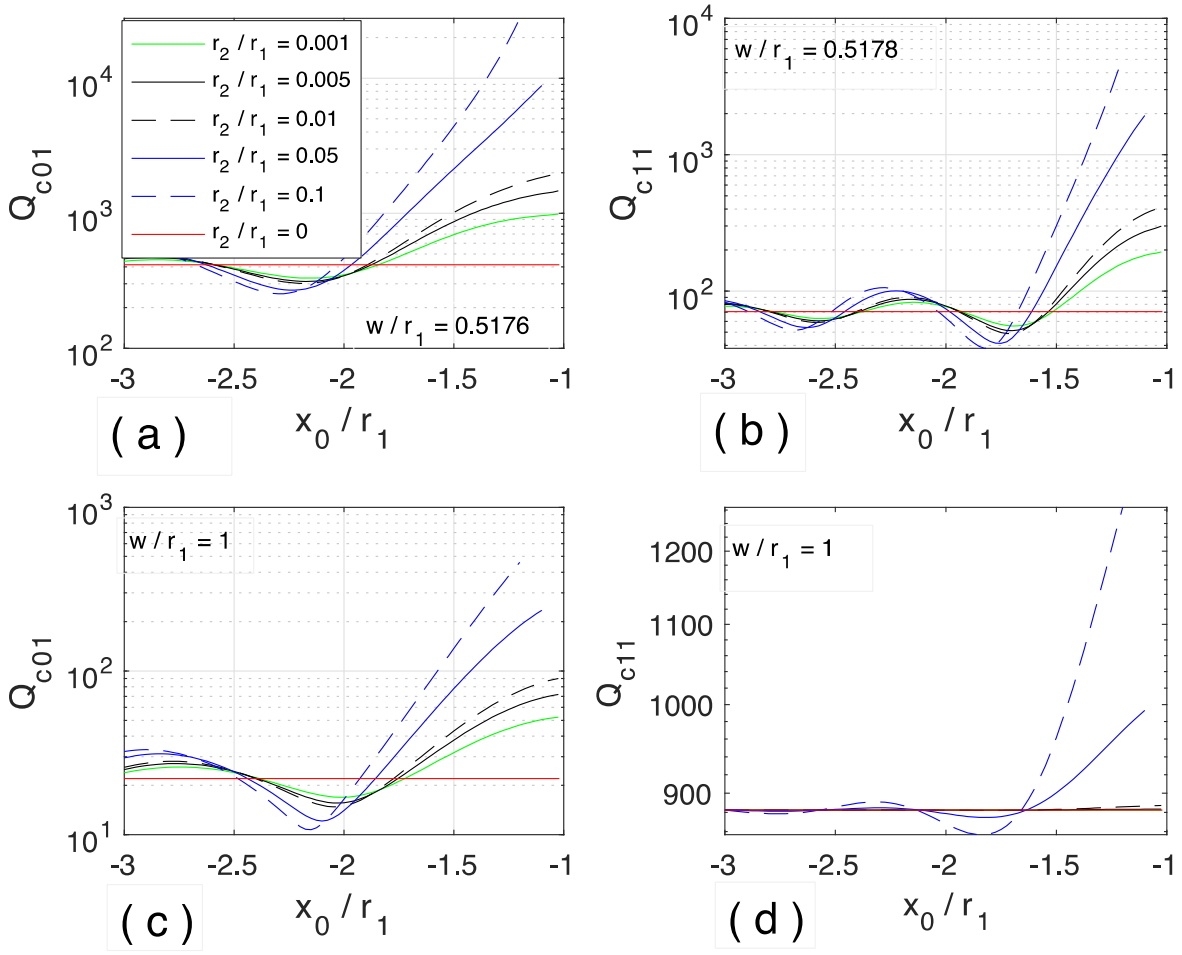

Figure 4. Q factor of the symmetric modes TM_{c01}, TM_{c11} versus relative distance x_0/r_1 for slotted cavities ($w/r_1 \approx 0.5176,\ 1$) in a presence of outside wires ($r_2/r_1 = 0.001,\ 0.005, 0.01$) and thin circular cylinders ($r_2/r_1 = 0.05,\ 0.1$): (**a**) Q_{c01}, $w/r_1 \approx 0.5176$; (**b**) Q_{c11}, $w/r_1 \approx 0.5176$; (**c**) Q_{c01}, $w/r_1 = 1$; (**d**) Q_{c11}, $w/r_1 = 1$.

This assertion becomes more obvious if we introduce the *enhancement coefficient*

$$\eta_{c(s)nm} = Q_{c(s)nm}/Q^{(0)}_{c(s)nm} \tag{6}$$

of the Q factor, where $Q^{(0)}_{c(s)nm}$ describes the resonance oscillations in the isolated cavity, and $Q_{c(s)nm}$ in system "cavity-rod". The enhancement coefficient was calculated for two eigenmodes TM_{c01} and TM_{s11} at relative positions $x_0/r_1 = -1.001 - r_2/r_1$

$(r_2/r_1 = 0.001,\ 0.005,\ 0.01,\ 0.05,\ 0.1)$ and relative slit widths $w/r_1 = 0.5176, 1$. In addition, the real parts γ'_{c01} and γ'_{s11} of the complex eigenvalues were calculated with an accuracy of six significant decimal digits and are displayed in Table 3. These data are useful when studying the resonance scattering when $kr_1 = \gamma'_{c(s)nm}$. Taking into account the multi-parameter nature of the problem, we selected parameters which best illustrate the basic properties of a resonance system. This, undoubtedly, arose from locating the wire (rod) in the closest possible proximity to the slit at relative distance $x_0/r_1 = -1.001 - r_2/r_1$ (see Table 3).

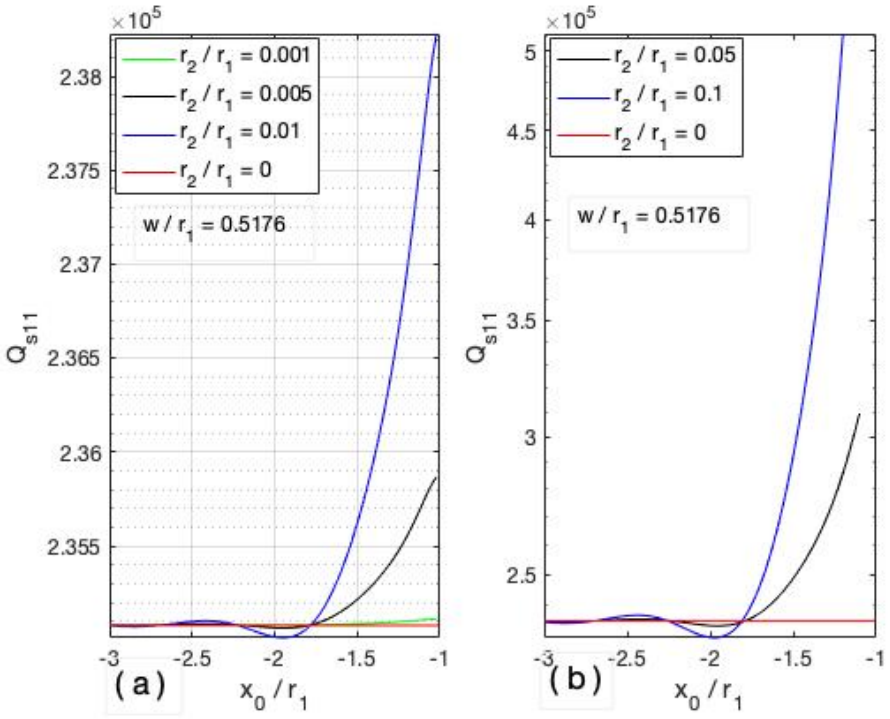

Figure 5. Q factor of anti-symmetric mode TM_{s11} versus relative distance x_0/r_1 for slotted cavity $(w/r_1 \approx 0.5176)$ with outside: (**a**) wires $(r_2/r_1 = 0.001,\ 0.005,\ 0.01)$; (**b**) thin circular cylinders $(r_2/r_1 = 0.05\ ,\ 0.1)$.

Table 3. Influence of the PEC rod on complex eigenvalues of the open circular cavity.

r_2/r_1	w/r_1=2sinπ/12≈0.5176 η_{c01} (Upper) γ'_{c01} (Lower)	w/r_1=2sinπ/12≈0.5176 η_{s11} (Upper) γ'_{s11} (Lower)	w/r_1=2sinπ/6=1 η_{c01} (Upper) γ'_{c01} (Lower)	w/r_1=2sinπ/6=1 η_{s11} (Upper) γ'_{s11} (Lower)
0.001	2.46 2.389066	1.00 3.831095	2.39 2.333257	0.990 3.819452
0.005	3.64 2.391529	1.00 3.831096	3.30 2.342239	0.993 3.819459
0.01	4.91 2.392912	1.01 3.831098	4.13 2.347373	0.997 3.819479
0.05	25.80 2.396639	1.35 3.831144	11.64 2.362121	1.128 3.819961
0.1	156.24 2.398246	3.01 3.831203	29.57 2.369028	1.558 3.820811

Let us turn to the calculation of the jump of surface current densities (SCDs), $\sigma_c(\phi)$ and $\sigma_r(\phi)$, on the walls of the cavity and the wire (rod), respectively (note that the angle ϕ corresponds to that of the polar coordinate system (ρ, ϕ, z)). We extracted the relevant data from Tables 2 and 3, and in addition, used the parameters $r_2/r_1 = 0.001,\ 0.01$ (wire) and

$r_2/r_1 = 0.1$ (rod). The SCDs $\sigma_c(\phi)$ and $\sigma_r(\phi)$ when the relative wave number kr_1 coincides with the real parts of the complex eigenvalues attributed to the TM_{c01} and TM_{s11} complex eigenmodes ($kr_1 = \gamma'_{c01}$ and $kr_1 = \gamma'_{s11}$) are shown in Figures 6 and 7, respectively. The most effective excitation of the TM_{c01} mode occurs at the incident angle $\alpha = 0°$ while for the TM_{s11} mode, it occurs at $\alpha = 45°$. The plots in Figures 6 and 7 match the corresponding SCD $\sigma_c(\phi)$ of the *closed* cylindrical cavity well except in the proximity of the sharp edges: the *edge effect* is responsible for the enormous growth in the SCD at the edges of the cavity. The magnitude of the resonant SCD values may be fully appreciated upon recognising that, in the *non-resonant case*, the value $\sigma_c(\phi)$ lies within the interval $0 < \sigma_c(\phi) < 3$.

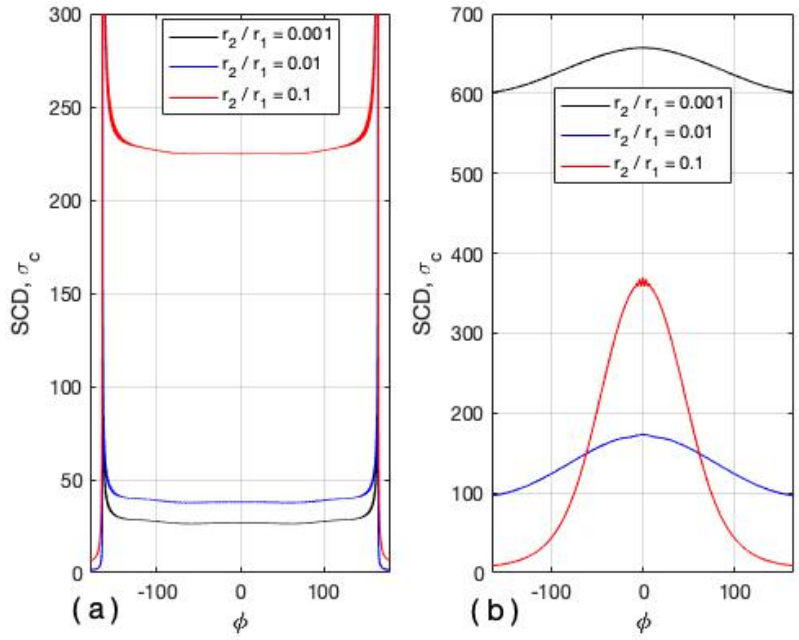

Figure 6. Surface current density (SCD) $\sigma_c(\phi)$ for resonant excitation of the TM_{c01} complex eigenmode over: (**a**) the cavity surface ($-165° \leq \phi \leq 165°$, $\phi_0 = \pi/12$); (**b**) the rod surface ($-\pi \leq \phi \leq \pi$).

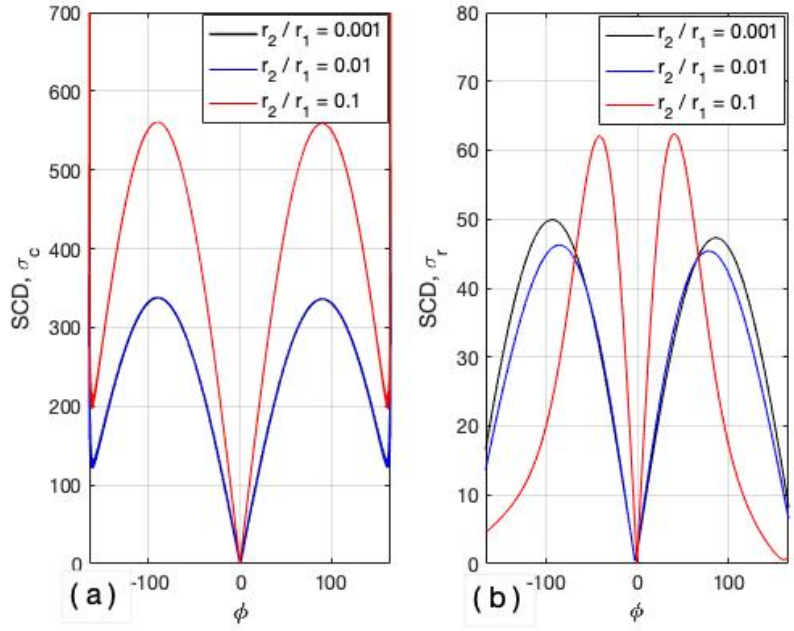

Figure 7. Surface current density (SCD) at the resonant excitation of the TM_{s11} complex eigenmode over: (**a**) the cavity surface ($-165° \leq \phi \leq 165°$, $\phi_0 = \pi/12$); (**b**) the rod surface ($-\pi \leq \phi \leq \pi$).

The next figure (Figure 8) illustrates why we pursued high accuracy in the calculation of the real parts of the complex eigenvalues $\gamma'_{c(s)nm}$, determining them with an accuracy of six significant decimal digits. When the cavity–rod system is excited at the resonant frequency (in our case, at the relative wave number $kr_1 = \gamma'_{c01}$), the value γ'_{c01} may be found with differing precisions. If we use the following set of parameters—$r_2/r_1 = 0.1$, $x_0/r_1 = -1.101$ and $w/r_1 = 2\sin\pi/12 \approx 0.5176$—then, according to Table 3, we may predict resonant excitation of the complex eigenmode TM_{c01} at $kr_1 = \gamma'_{c01} = 2.398246$; the corresponding maximum value of the SCD is $\max\limits_{\phi}\sigma_c(\phi) \approx 228$. Now, suppose that the precision of the value γ'_{c01} is successively reduced from six significant decimal digits to five, four, and three significant decimal digits so that excitation occurs at the relative wavenumbers $kr_1 = \gamma'_{c01} = 2.39824$, 2.3982, and 2.398. Upon recalculating the corresponding SCD $\sigma_c(\phi)$, it can be seen that the corresponding maxima drop to $\max\limits_{\phi}\sigma_c(\phi) \approx 214$, 85, and 20 respectively.

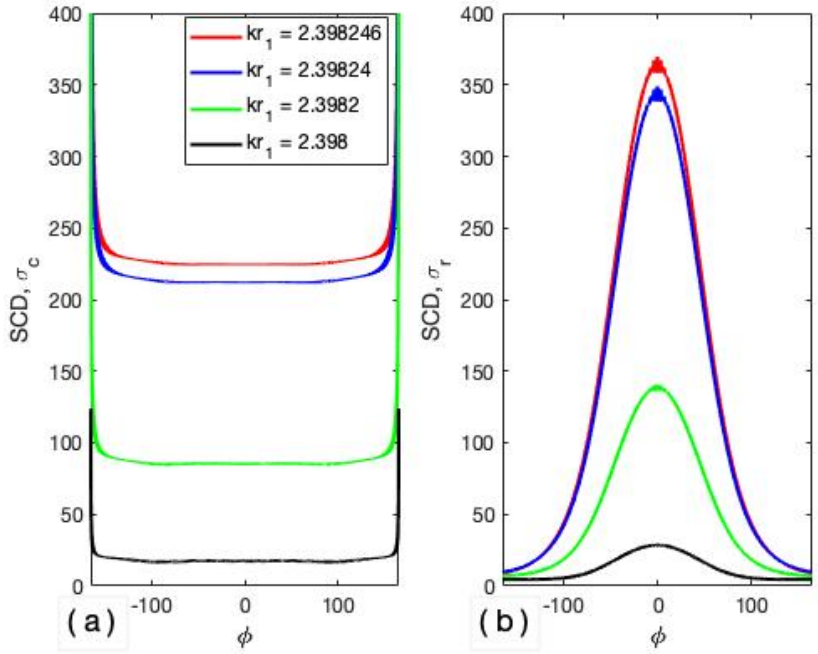

Figure 8. SCDs $\sigma_c(\phi)$ and $\sigma_r(\phi)$ under excitation of the TM_{c01} complex mode in the cavity–rod system ($r_2/r_1 = 0.1$, $x_0/r_1 = -1.101$, and $w/r_1 = 2\sin\pi/12 \approx 0.5176$): (**a**) cavity; (**b**) rod.

These data show, at least from a theoretical point of view, the importance of accurate calculation of the complex eigenvalues. In practice, it is also important, but advanced accuracy is less important because fine tuning of a resonator may be realised by changing the frequency of the generator, and when it is asserted that, for example, "four digits accuracy is reasonable for practice", it is difficult not to agree with such an assertion.

4. Electromagnetic Impact of the Circular Rod on a Rectangular Cavity with Longitudinal Slit

From the basics of waveguide theory, it is well-known that the cut-off wave numbers k_c of a rectangular cavity with sides a and b are given by

$$k_c = \sqrt{\left(\frac{m\pi}{a}\right)^2 + \left(\frac{n\pi}{b}\right)^2} \tag{7}$$

where the integers $n, m \neq 0$ $(n, m = 1, 2, \ldots)$. If we treat the metallic rectangular cavity as a cavity resonator, the same Formula (7) describes in terms of wave numbers the eigenvalues of standing harmonics (eigenmodes). Furthermore, we may use the dimensionless eigenvalues

$$\gamma_{mn}^{(0)} \equiv k_{mn}a = \pi\sqrt{m^2 + \left(\frac{a}{b}\right)^2 n^2} \tag{8}$$

where $b \geq a \geq$, $n, m = 1, 2, \ldots$ In the context of this paper, we restricted ourselves to finding the first three complex eigenvalues for the isolated ($r_2 = 0$) cavity with aspect ratio $b/a = 2$ and longitudinal slits of relative widths $w/a = 0.05,\ 0.2,$ and 0.5 using the methodology developed in [16]. These values are displayed in Table 4.

Table 4. Complex eigenvalues γ_{mn} of the isolated slotted rectangular cavity.

TM_{mn}	$w/a = 0$	$w/a = 0.1$	$w/a = 0.25$	$w/a = 0.5$
TM_{11}	3.512407	$3.510998 - i \cdot 8.578 \times 10^{-6}$	$3.502968 - i \cdot 3.9236 \times 10^{-4}$	$3.469693 - i \cdot 8.7565 \times 10^{-3}$
TM_{12}	4.442882	$4.438381 - i \cdot 4.4703 \times 10^{-5}$	$4.411898 - i \cdot 2.1270 \times 10^{-3}$	$4.305618 - i \cdot 4.3447 \times 10^{-2}$
TM_{13}	5.663586	$5.655510 - i \cdot 1.3348 \times 10^{-4}$	$5.605974 - i \cdot 6.7413 \times 10^{-3}$	$5.429296 - i \cdot 1.1579 \times 10^{-1}$

From a physical point of view, the replacement of a circular cavity by one of rectangular shape does not affect the emergence of the effect of Q factor enhancement when the rod (or wire) approaches the aperture of the rectangular cavity from inside. First, we calculated the Q factor dependence on relative distance x_0/a for all three complex eigenmodes ($TM_{11},\ TM_{12}$, and TM_{13}) using the parameters $b/a = 2$, $w/a = 0.25$, and $r_0/a = 0.025$. The Q factors $Q_{TM_{11}}(x_0/a)$, $Q_{TM_{12}}(x_0/a)$, and $Q_{TM_{13}}(x_0/a)$ were calculated in the interval $x_0/a \in (-5, -1.026) \cup (-0.974,\ 0.974) \cup (1.026,\ 5)$; they are plotted in Figure 9.

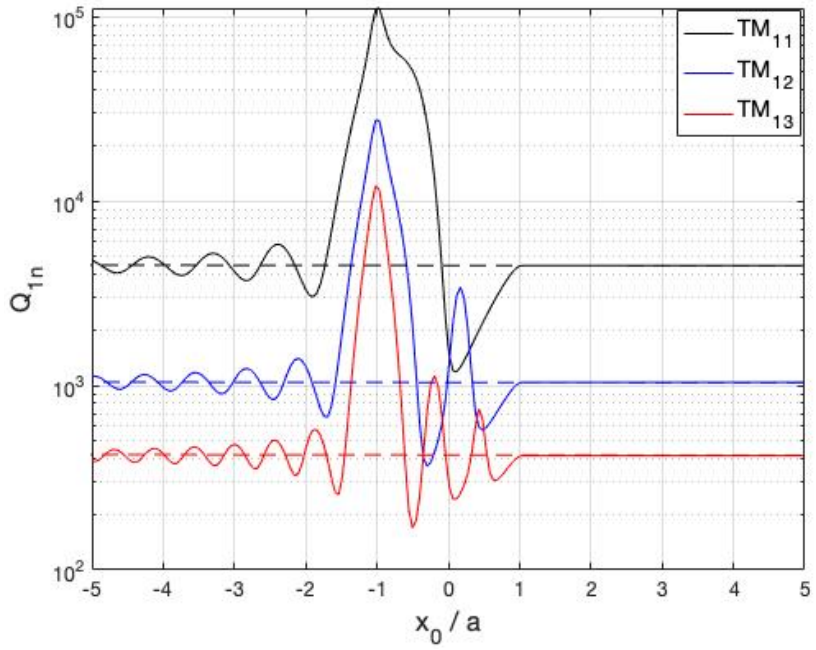

Figure 9. Q factor $Q_{TM_{1n}}(n = 1, 2, 3)$ versus relative distance x_0/a ($b/a = 2$, $w/a = 0.25$, and $r_0/a = 0.025$).

In Figure 9, the dashed lines are the values of the Q factors of the $TM_{11},\ TM_{12}$, and TM_{13} complex eigenmodes, calculated for isolated slotted rectangular cavities. Qualitatively, the behaviour of these plots is the same as that for the plots of $Q_{c01}(x_0/r_1)$ and $Q_{s11}(x_0/r_1)$ in the circular cavity (see Figure 3). We should note that in discussing the phenomenon of Q factor enhancement, the condition $2r_2/w \ll 1$ should be fulfilled: otherwise, if r_2/w is of the same order as w/r_1 or w/a, such enhancement is a rather trivial phenomenon, simply because the thick rod blocks the slit, making the cavity practically closed.

Figure 10 presents the calculation of the Q factor of the complex eigenmodes (TM_{11}, TM_{12}) versus relative distance x_0/a for rectangular slotted cavities ($w/a = 0.25,\ 0.5$) with wires ($r_2/a = 0.001,\ 0.005,\ 0.01$) and thin circular cylinders ($r_2/a = 0.05,\ 0.1$).

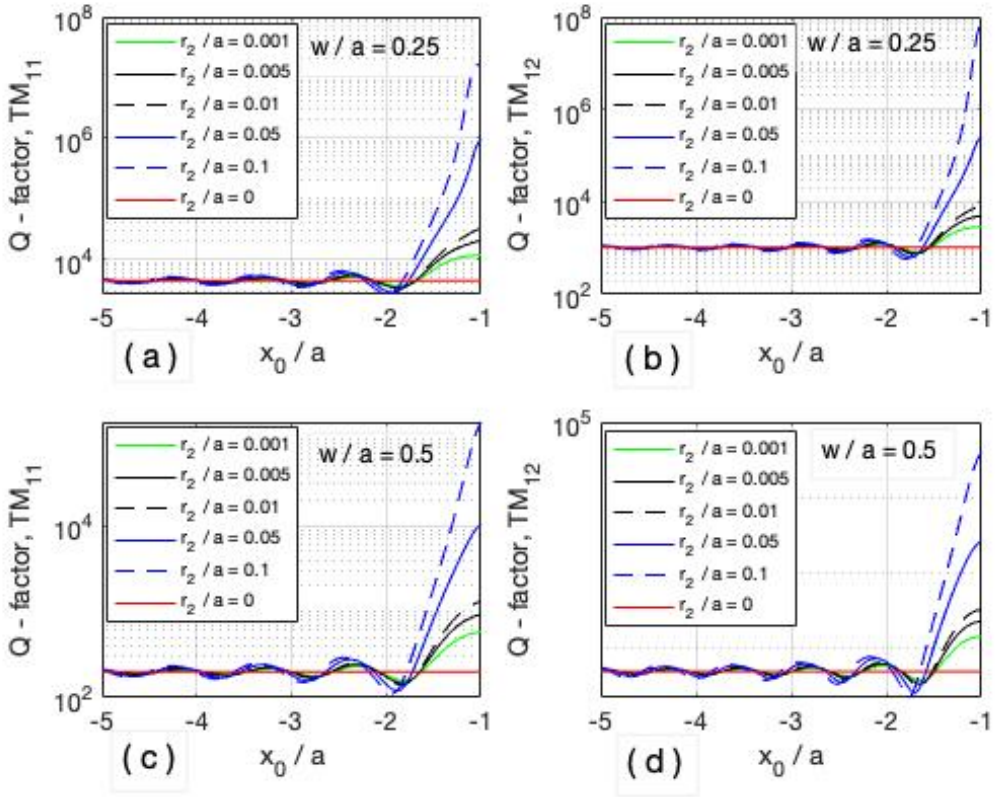

Figure 10. Q factor of complex eigenmodes (TM_{11}, TM_{12}) versus relative distance x_0/a for rectangular slotted cavities with wires ($r_2/a = 0.001,\ 0.005,\ 0.01$) and thin circular cylinders ($r_2/a = 0.05,\ 0.1$): (**a**) Q_{11}, $w/a = 0.25$; (**b**) Q_{12}, $w/a = 0.25$; (**c**) Q_{11}, $w/a = 0.5$; (**d**) Q_{12}, $w/a = 0.5$.

The corresponding calculations for the complex eigenmode TM_{13} with wires are presented in Figure 11. The enhancement due to thin rods ($r_2/a = 0.05,\ 0.1$) was omitted, but it is huge and may be simply estimated from these plots. We concentrated on the electromagnetic interaction between the slotted cavity and wires ($r_2/a = 0.001,\ 0.005,\ 0.01$).

Let us consider a typical rectangular waveguide, for example, WR159 (EIA Standard), specified by the dimensions 1.59 inches (40.386 mm) by 0.795 inches (20.193 mm). The corresponding parameters in this paper are $a = 20.193$ mm, $b = 40.386$ mm ($b/a = 2$), and $w = 5.048$ mm ($w/a = 0.25$) or $w = 10.096$ mm ($w/a = 0.5$). The diameter of the wire ($2r_2$) can then be determined from its aspect ratio r_2/a, giving $2r_2 = 0.04$ mm ($r_2/a = 0.001$), 0.2 mm ($r_2/a = 0.005$), or 0.4 mm ($r_2/a = 0.01$). There is no need to specify the precise type of copper wire as wires of such diameter can be readily found in numerous handbooks on electro- or radio engineering. This waveguide example shows the relevance of the parameters used in this paper to electro-engineering practice. The enhancement by thin wires of the Q factor may be seen in the data displayed in Table 5. In this Table, the quantities Δ_{1n} ($n = 1, 2, 3$) represent the shifts in the real parts of the complex eigenvalues which occur when the rods (or wires) are coupled to isolated slotted rectangular cavities. The non-perturbed complex eigenvalues for isolated cavities were extracted from Table 4 for cavities with relative widths $w/a = 0.25$ and $w/a = 0.5$.

Table 5 also contains the *enhancement coefficients* η_{1n} ($n = 1, 2, 3$), defined in a similar way to that in Equation (6): $\eta_{1n}(x_0/a) = Q_{1n}(x_0/a)/Q_{1n}^{(0)}$, where the superscript zero refers to the TM_{1n} complex eigenmodes emerging in the isolated slotted rectangular cavity. The position of the wire was fixed at the points $x_0/a = -1.001 - r_2/a$, where $r_2/a = 0.001,\ 0.005,\ 0.01$, so that the parameter x_0/a takes the values -1.002, -1.006, and -1.011. All the shifts Δ_{1n} ($n = 1, 2, 3$)

are positive and tend to grow as the thickness of the wire increases and as the oscillation number n across the wider side b of the slotted rectangular cavity increases. In terms of the above-mentioned WR159 (EIA Standard) waveguide, the value of the relative parameter $r_2/a = 0.001$ physically corresponds to the minimum diameter of a human hair. Taking this into account, perhaps there is no exaggeration in characterizing the Q factor enhancement of 2.5 to 3 times by such a thin wire as a *striking effect*.

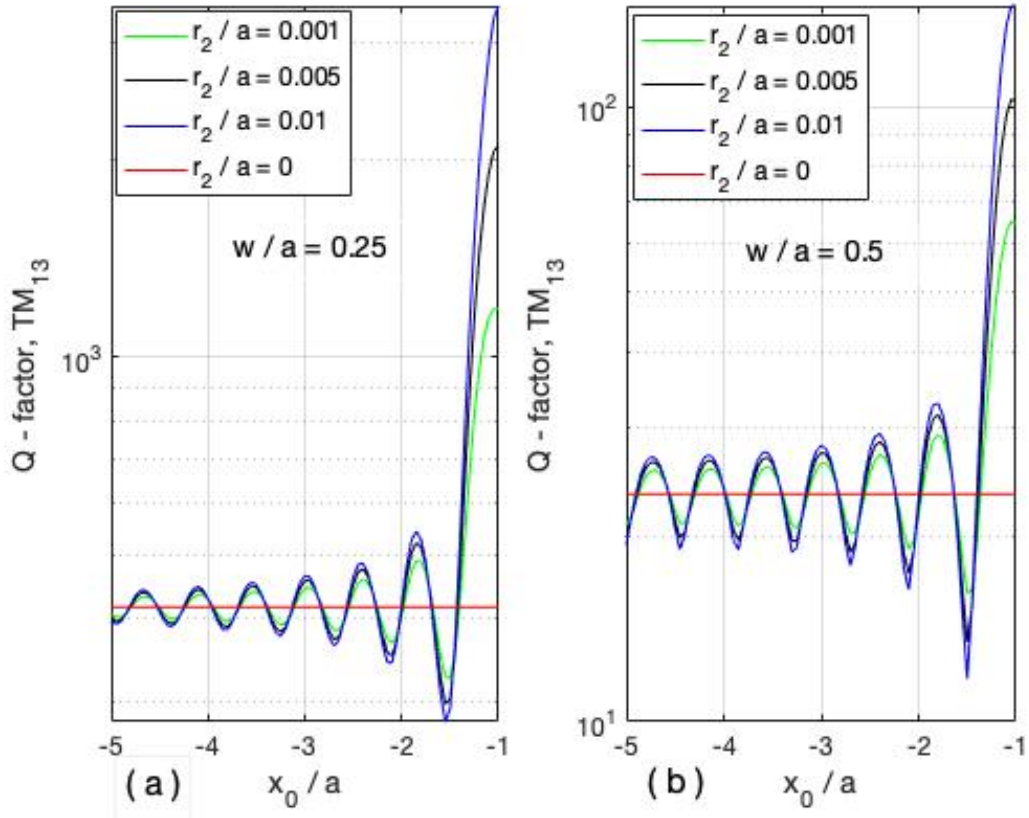

Figure 11. Q factor of the complex eigenmode TM_{13} versus relative distance x_0/a for rectangular slotted cavities with wires $(r_2/a = 0.001,\ 0.005,\ 0.01)$: (**a**) $w/a = 0.25$; (**b**) $w/a = 0.5$.

Table 5. Enhancement coefficients η_{1p} and real parts of the shifts $\Delta_{1p}(p = 1, 2, 3)$ for complex eigenvalues of slotted $(w/a = 0.25,\ 0.5)$ rectangular cavity in a presence of the wires $(r_2/a = 0.001,\ 0.005,\ 0.01)$.

TM_{1n}	TM_{11}		TM_{12}		TM_{13}	
			w/a = 0.25			
r_2/a	Δ_{11}	η_{11}	Δ_{12}	η_{12}	Δ_{13}	η_{13}
0.001	0.003653	2.732	0.012272	2.824	0.023526	2.953
0.005	0.004793	4.811	0.016044	5.032	0.030607	5.363
0.01	0.005408	7.843	0.018069	8.291	0.034377	8.970
			w/a = 0.5			
r_2/a	Δ_{11}	η_{11}	Δ_{12}	η_{12}	Δ_{13}	η_{13}
0.001	0.017761	2.958	0.056446	2.906	0.091508	2.786
0.005	0.022462	4.715	0.071723	4.658	0.117458	4.454
0.01	0.025018	6.716	0.080064	6.683	0.131827	6.406

We conclude this Section with an instructive example of resonance excitation, calculating the SCD $\sigma_c(\phi)$ on the surface of the rectangular cavity and the SCD distribution $\sigma_r(\phi)$ over the cylindrical surface of the wire. For the rectangular cavity, the angular parameter ϕ relates to an arc length parameter which is used for parameterisation of the cavity boundary. We excited all three (TM_{11}, TM_{12}, TM_{13}) complex eigenmodes using excitation angle $\alpha = 0^0$. The relevant parameters were extracted from the Table 5 for the relative slit width $w/a = 0.25$. The results of calculations are presented in Figure 12 (TM_{11}), Figure 13 (TM_{12}), and Figure 14 (TM_{13}). The SCD distribution $\sigma_c(\phi)$ along the rectangular cavity displays anticipated behaviour including growth of the resonant value as the relative radius varies, and strong similarity of the EMF structure of each mode to that of the canonical EMF structure corresponding to the closed cavity mode characterised, for example, by the same number of field variations along the wider (length b) and narrower (length a) walls of the rectangular cavity, is observed. This similarity to the canonical EMF modal structure is distorted only in the proximity of the sharp edges of the slit.

An apparent contradiction arises in the behaviour of the SCD distribution $\sigma_c(\phi)$ over the surface of the rod (or wire), where the growth of the Q factor (as the rod thickens) is associated with a decrease in the SCD $\sigma_r(\phi)$. It may be resolved in the following way. Any corner of a conductor, even after rounding off with a small radius of curvature $r_2 \ll \lambda$, interacts with the electromagnetic field as though it were a sharp edge, giving rise to a significant but finite increase in the surface current density. The same is true for the wire, and as its diameter $2r_2$ increases, the magnitude of this effect steadily reduces; this is precisely what is observed in the plots $\sigma_r(\phi)$, calculated for different values of the relative thickness r_2/a of the wire.

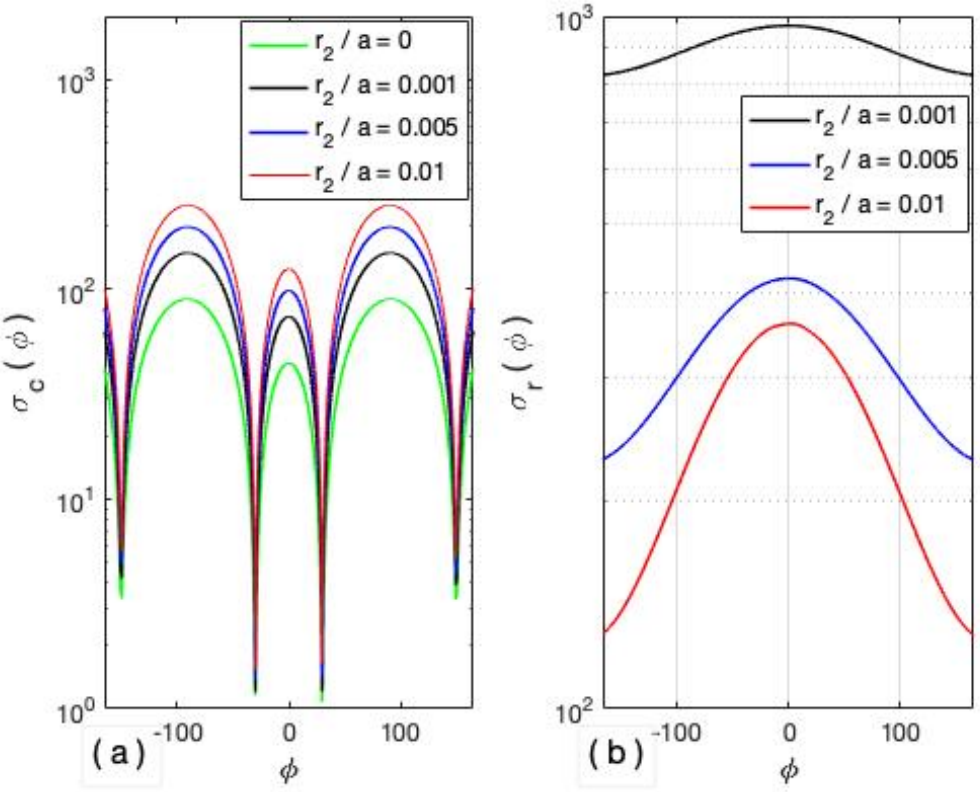

Figure 12. SCD distribution $\sigma_c(\phi)$ and $\sigma_r(\phi)$ under excitation of the TM_{11} mode (w/a = 0.25): (**a**) cavity; (**b**) rod.

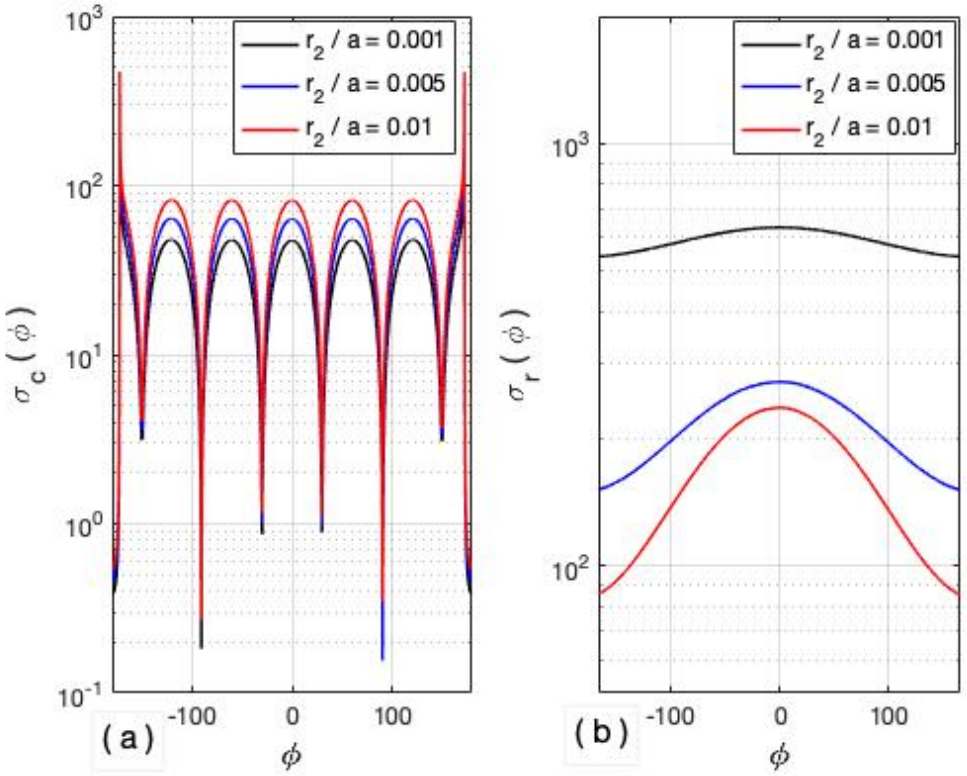

Figure 13. SCD distribution $\sigma_c(\phi)$ and $\sigma_r(\phi)$ under excitation of the TM_{12} mode (w/a = 0.25): (**a**) cavity; (**b**) rod.

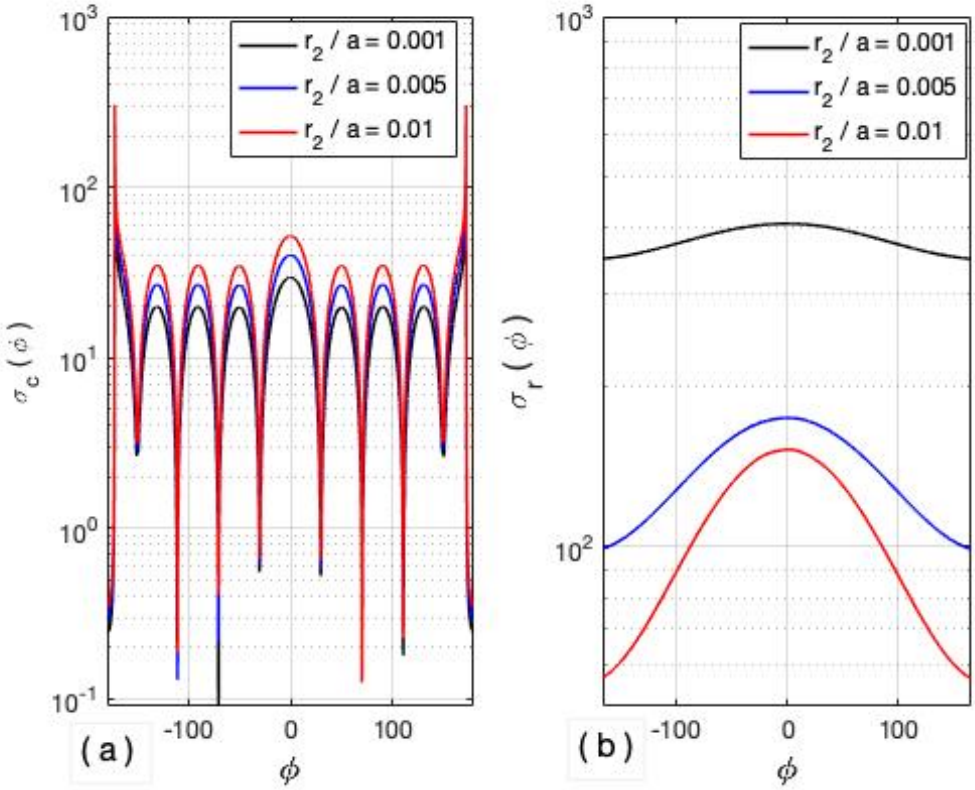

Figure 14. SCD distribution $\sigma_c(\phi)$ and $\sigma_r(\phi)$ under excitation of the TM_{13} mode (w/a = 0.25): (**a**) cavity; (**b**) rod.

5. Conclusions

The scattering of an obliquely propagating *E*-polarized plane wave by the coupled structure consisting of a 2D cavity and metallic rod was rigorously solved. The problem was posed as a classical mixed boundary value problem for Maxwell's equations, and after application of the method of analytical regularization, a coupled set of well-conditioned matrix equations of the second kind was obtained. The fast convergence of the solution to the truncated system of equations to the exact solution as the truncation order is increased was demonstrated. This was the basis for our studies of electromagnetic coupling between a circular rod and slotted circular or rectangular cavities.

The spectral characteristics of these open cavities in the presence of a circular rod (or wire) was examined for the first three complex eigenmodes for the longitudinally slotted circular cavity (namely, TM_{c01}, TM_{c11}, TM_{s11}) and for the slotted rectangular cavity (TM_{11}, TM_{12}, TM_{13}). The complex eigenvalues were calculated with an accuracy of six significant decimal digits. In particular, it was found that placement of a *thin* wire in close proximity to the slit may enhance the Q factor from two to eight times. Using the specifications of a certain standard waveguide used in practice, the thickness of the wire was shown to be comparable with that of a human hair. In addition, the resonant current distributions on the surfaces of the slotted cavity and the rod (or wire) were accurately calculated for a variety of parameters.

Whilst important in themselves, these highly accurate results may be used for validation of results obtained by other approximate methods that are often used for solving similar problems in electromagnetic coupling. It is natural to extend the study of coupling of a resonance cavity with a tuning element to consider *H*-polarization. In this case, the spectrum of complex natural oscillations include an additional type of low-frequency oscillation. Known as the Helmholtz mode in the acoustic case, in the electromagnetic case, this oscillation it is usually described as "an oscillation that is an electromagnetic analogue of that of the Helmholtz resonator." Whilst there have been publications employing similar ideas and techniques to those of the papers [1–8], in order to achieve benchmark solutions of quality matching the *E*-polarization case discussed in this paper, the MAR or one of its variants should be used. In this case, there is significant additional complexity due to the hypersingular nature of the kernel obtained in the process of formulation with double layer potentials. In another direction, arrays of suitably tuned cavity elements offer possibilities for beam steering in either polarisation.

Author Contributions: Both authors (E.D.V. and P.D.S.) contributed equally to the manuscript, in its conceptualisation, methodology, formal analysis, investigation, and validation, and in the writing, reviewing, and editing of the manuscript; E.D.V. developed the software code. All authors have read and agreed to the published version of the manuscript..

Funding: This research received no external funding.

Data Availability Statement: Not applicable.

Conflicts of Interest: The authors declare no conflict of interest.

References

1. Bopp, C.L.; Butler, C.M. Efficient Methods for Determining the Coupling to Wires in Circular Cavities. *IEEE Trans. Electromagn. Compat.* **2007**, *49*, 382–390. [CrossRef]
2. Tkachenko, S.V.; Rambousky, R.; Nitsch, J.B. Electromagnetic Field Coupling to a Thin Wire Located Symmetrically Inside a Rectangular Enclosure. *IEEE Trans. Electromagn. Compat.* **2013**, *55*, 334–341. [CrossRef]
3. Elnaggar, S.Y.; Tervo, R.J.; Mattar, S.M. Coupled Mode Theory Applied to Resonators in the Presence of Conductors. *IEEE Trans. Microw. Theory Tech.* **2015**, *63*, 2124–2132. [CrossRef]
4. Rabat, A.; Bonnet, P.; Drissi, K.E.K.; Girard, S. Analytical Models for Electromagnetic Coupling of an Open Metallic Shield Containing a Loaded Wire. *IEEE Trans. Electromagn. Compat.* **2017**, *59*, 1634–1637. [CrossRef]
5. Quedraogo, R.; Rothwell, E.; Chen, S.-Y.; Greetis, B. An Automatically Tunable Cavity Resonator System. *IEEE Trans. Microw. Theory Tech.* **2010**, *58*, 894–902. [CrossRef]

6. Lee, J.-I.; Lee, C.-H.; Cho, Y.-K. Electromagnetic Coupling Mechanism to a Conducting Strip Through a Narrow Slit in a Parallel-Plate Waveguide. *IEEE Trans. Antennas Propag.* **2001**, *49*, 592–596.
7. Lail, B.A.; Castillo, S.P. Coupling Through Narrow Slot Apertures to Thin-Wire Structures. *IEEE Trans. Electromagn. Compat.* **2000**, *42*, 276–283. [CrossRef]
8. Butler, C.M.; Umashankar, K.R. Electromagnetic excitation of a wire through an aperture-perforated conducting screen. *IEEE Trans. Antennas Propagat.* **1976**, *24*, 456–462. [CrossRef]
9. Hsiao, G.C.; Kleinman, R.E. Mathematical foundations for error estimation in numerical solutions of integral equations in electromagnetics. *IEEE Trans. Antennas Propag.* **1997**, *45*, 316–321. [CrossRef]
10. Vinogradov, S.S.; Smith, P.D.; Vinogradova, E.D. *Canonical Problems in Scattering and Potential Theory. Part I. Canonical Structures in Potential Theory*; Chapman & Hall/CRC: Boca Raton, FL, USA, 2001; p. 374.
11. Vinogradov, S.S.; Smith, P.D.; Vinogradova, E.D. *Canonical Problems in Scattering and Potential Theory. Part II. Acoustic and Electromagnetic Diffraction by Canonical Structures*; Chapman & Hall /CRC: Boca Raton, FL, USA, 2002; p. 501.
12. Lucido, M.; Di Murro, F.; Panariello, G. Electromagnetic Scattering from a Zero-Thickness PEC Disk: A Note on the Helmholtz-Galerkin Analytically Regularizing Procedure. *Prog. Electromagn. Res. Lett.* **2017**, *71*, 7–13. [CrossRef]
13. Oguzer, T.; Nosich, A.I.; Altintas, A. E-polarized beam scattering by an open cylindrical PEC strip having an arbitrary "conical-section" profile. *Microw. Opt. Technol. Lett.* **2001**, *31*, 480–484. [CrossRef]
14. Vinogradova, E. Electromagnetic Plane Wave Scattering by Arbitrary Two-Dimensional Cavities: Rigorous Approach. *Wave Motion* **2017**, *70*, 47–64. [CrossRef]
15. Vinogradova, E.D. Scattering of E Polarized Plane Wave by Rectangular Cavity with Finite Flanges. *Radio Sci.* **2017**, *52*, 1374–1385. [CrossRef]
16. Vinogradova, E.D. Complex Eigenvalues of Slotted Arbitrary Cylindrical Cavities: Sound-Soft Elliptic Cavity with Variably Placed Longitudinal Slit. *J. Acoust. Soc. Am.* **2018**, *144*, 1146. [CrossRef] [PubMed]
17. Safonova, G.; Vinogradova, E. Accurate Backscattering Studies for Double-Layered Array of Infinitely Long Cylinders. *Microw. Opt. Technol. Lett.* **2013**, *55*, 2127–2131. [CrossRef]
18. Safonova, G.; Vinogradova, E.; Tuchkin, Y. Accurate Impedance Calculations for Transmission Lines with Adjustable Inner Conductor. *Microw. Opt. Technol. Lett.* **2014**, *56*, 2066–2070. [CrossRef]